

## **High-Field/High-Frequency EPR Spectrometer Operating in Pulsed and Continuous-Wave Mode at 180 GHz**

**M. Rohrer\*, O. Brüggemann, B. Kinzer, and T. F. Prisner**

Institute of Physical and Theoretical Chemistry, University of Frankfurt, Frankfurt/Main, Germany

Received July 12, 2001

**Abstract.** A novel electron paramagnetic resonance (EPR) spectrometer is reported, which has been developed to allow pulsed EPR experiments with high sensitivity and time resolution at a microwave (MW) frequency of 180 GHz (G-band) and wavelengths of approximately 1.6 mm. This corresponds to a magnetic field of about 6.4 T for  $g \approx 2$  signals. The “hybrid” system architecture combines components of quasioptical as well as conventional MW techniques, making it possible to achieve excellent spectrometer performance with respect to sensitivity and time resolution. Quasioptical MW components have been used to design an MW circulator allowing high sensitivity and low bias operation in the reflection mode. A miniaturized, closed-type cylindrical cavity provides a high sample filling factor and an adequate MW field strength ( $B_1$ ) enhancement and thus permits reasonably short MW pulses (60 ns for a  $\pi/2$  pulse) even with a moderate MW input power (15 mW at the cavity). Commercial quartz capillaries (up to 0.5 mm internal diameter) can be used as sample holders for a broad range of applications.

### **1 Introduction and Motivation**

During the previous decade an increasing number of high-field/high-frequency electron paramagnetic resonance (HF-EPR) spectrometers have been developed operating in continuous-wave (CW) [1–6] or in the pulsed mode [7–11], reflecting the potential offered by this technique. Applications of HF-EPR range from semiconductor materials [12] and inorganic coupled spin cluster systems [13, 14] to transition metal centers [15–19] and organic radicals in proteins [20–24].

Advantages of HF-EPR spectroscopy for high-spin systems are twofold: integer spin systems, that are “EPR-silent” at traditional EPR fields (X-band, 0.3 T) as a result of their large zero-field splitting become observable by HF-EPR [25] and, on the other hand, the central transition of half-integer spin-systems ( $m_S = -1/2 \leftrightarrow +1/2$ ) becomes substantially narrowed [26]. In Fig. 1, CW EPR spectra

---

\* Present address: SBU Diagnostics, Schering AG, Berlin, Germany.

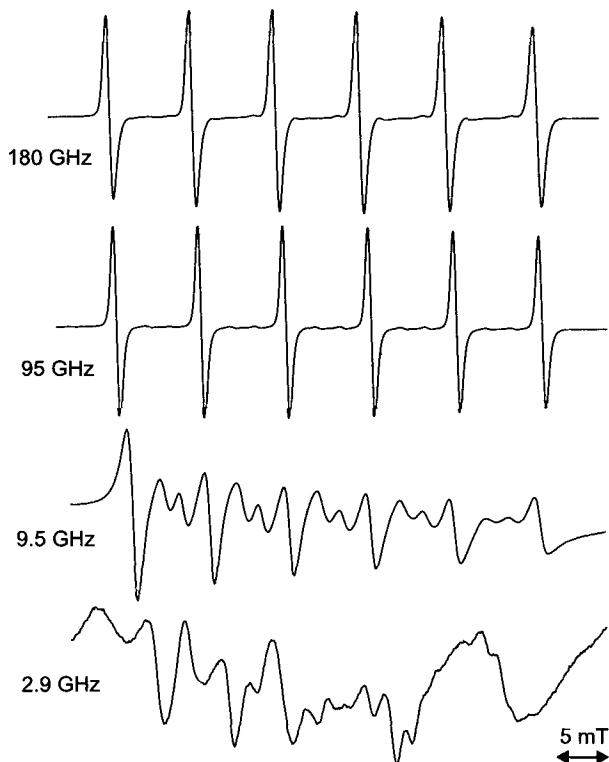


**Fig. 1.** Multifrequency CW EPR on the protein nucleotide complex  $p21^{\text{ras}} \cdot \text{Mn}^{2+} \cdot \text{GDP}$  in frozen solution. The increased spectral resolution for higher MW frequencies is due to two effects: first, the narrower linewidth of the  $m_s = -1/2 \leftrightarrow +1/2$  transition of systems with zero-field splitting, and second, the suppression of forbidden transitions with  $\Delta m_s = \pm 1$  and  $\Delta m_l = \pm 1$ .

of a protein-nucleotide complex with a  $\text{Mn}^{2+}$  metal ion ( $p21^{\text{ras}} \cdot \text{Mn}^{2+} \cdot \text{GDP}$ ) in frozen solution are shown at different microwave (MW) frequencies, illustrating the increased spectral resolution with increasing magnetic fields and MW frequencies. Naturally, the active center of this protein complex contains an  $\text{Mg}^{2+}$  ion, which can be exchanged to  $\text{Mn}^{2+}$  without significantly altering the biological activity of the protein [27]. The paramagnetic  $\text{Mn}^{2+}$  ion ( $S = 5/2$ ,  $I = 5/2$ ) gives rise to six lines in CW EPR spectra of disordered samples. Specific point mutants of the  $p21^{\text{ras}}$  protein, as they can be found in human cancer cells, lead to a reduction or inhibition of the catalytic reaction that takes place at the active metal site of the protein complex. The increased resolution of the HF-EPR spectra allows a more detailed investigation of the structural and conformational changes of these different mutants [19].

The small  $g$ -anisotropy of organic radicals, as, for example, semiquinone anion radicals, can only be resolved at high magnetic fields, offering increased information especially for disordered powder samples. Quinones occur in many protein complexes and play an important role for charge transfer processes through

biological membranes. In Fig. 2, the X-band and G-band (180 GHz, 6.4 T) CW EPR spectra of vitamin K<sub>3</sub> (a naphthoquinone derivative) are shown. The spectra clearly demonstrate the increased resolution of anisotropic  $g$ -tensors at higher magnetic fields, which can be used to obtain orientation-dependent information about the system under study. For example, this can be structural information on the local protein environment around the semiquinone radical [20, 24, 28, 29] and, in conjunction with pulsed EPR methods, also information on the local dynamics [30].

Pulsed EPR at high magnetic fields can further increase spectral resolution [26, 31]. Overlapping spectra of different paramagnetic species can often be separated by differences in their relaxation times  $T_1$  or  $T_2$ . In solid or slow tumbling samples, small spectral contributions, as, for example, spin-spin couplings, are often unresolvable because of inhomogeneous broadening mechanisms. These contributions can be resolved by pulsed refocusing techniques. Whereas at X-band frequencies such techniques are widely used for the investigation of unresolved hyperfine couplings to closeby nuclei, the electron spin echo envelope modulation (ESEEM) depth for most nuclei will decrease strongly at high magnetic fields and therefore reduce the use of these methods at higher magnetic fields [32, 33]. On the other hand, the spectral resolution of anisotropic  $g$ -tensors at high magnetic fields allows one to perform orientationally selective pulsed EPR and electron nuclear double resonance (ENDOR) experiments. Therefore angular information on such quantities as anisotropic relaxation, librational motion [30], dipolar or hyperfine coupling tensors [29, 34] can be obtained. As an example for anisotropic relaxation times  $T_2$ , two-pulse echo-detected spectra at an MW frequency of 180 GHz of a TEMPO (2,2,6,6-tetramethyl-1-piperidinyloxy) spin label are shown in Fig. 3. Nitroxide radicals are widely used with site-specific spin-labelling techniques to gain increased information on structural and dynamical proper-

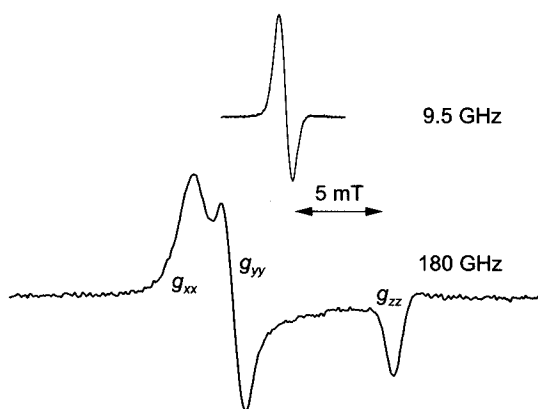


**Fig. 2.** CW EPR spectra on vitamin K<sub>3</sub> in 2-butanol in frozen solution ( $T = 20$  K). In the upper trace a CW X-band spectrum is shown, where only one unresolved EPR line can be seen. In the lower trace a CW G-band ( $\nu = 180$  GHz,  $B_{\text{center}} = 6.43$  T) spectrum is shown, where the anisotropy of the  $g$ -tensor can clearly be resolved.

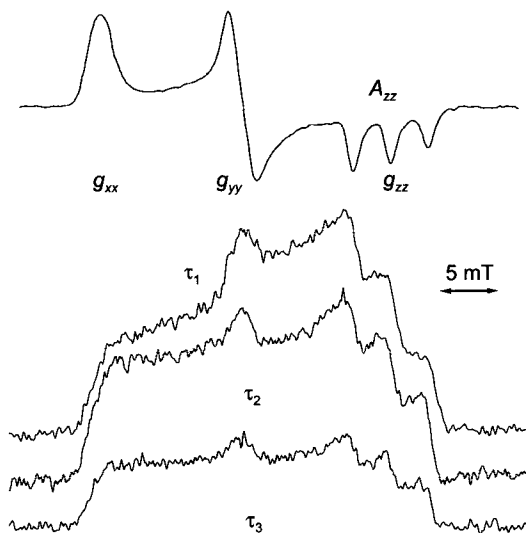


**Fig. 3.** Field-swept two-pulse echo spectra of TEMPO spin label in a polystyrene matrix at an MW frequency of 180 GHz ( $T = 40$  K). In the CW spectrum (upper trace) the well-resolved canonical peaks of the anisotropic  $g$ -tensor and the resolved nitrogen hyperfine coupling  $A_{zz}$  component can be easily seen. The echo-detected spectra recorded for different  $\tau$  values ( $\tau_1 = 100$  ns,  $\tau_2 = 200$  ns,  $\tau_3 = 400$  ns) demonstrate the anisotropic  $T_2$  relaxation time.

ties of biological macromolecules [35–38]. The spectra of nitroxide radicals are dominated by the well-resolved anisotropic  $g$ -tensor at high magnetic fields, which is not the case for X-band EPR spectra. In this example the  $g_{zz}$ -peak is split into three lines due to the large  $A_{zz}$  component of the hyperfine coupling tensor to the nitrogen nucleus ( $I = 1$ ). The change of the spectral shape for different pulse separation times  $\tau$  indicates the anisotropy of the relaxation time  $T_2$ .

While an increased MW frequency offers advantages for spectral resolution, it also makes great demands on the technical design of HF-EPR spectrometers. The most critical parts are the MW components for generation (a) and detection (b) of the high-frequency signals and pulses, the transfer of the MW pulses to the sample and the signal back to the detector (c), the MW resonator (d) and the magnetic field (e). For an overview about technical and theoretical aspects as well as applications of HF-EPR see, for example, ref. 26.

While CW HF-EPR can even be performed without a resonator in a single-pass transmission mode configuration [3, 6, 24], the implementation of a resonator is indispensable for pulsed EPR experiments in order to achieve reasonably short MW pulse lengths as compared to transverse relaxation times  $T_2$  of the spin systems. The size of fundamental-mode MW cavities scales reciprocally with their resonance frequency, making sample handling as well as MW coupling to the cavity more difficult at higher frequencies. Nevertheless, closed-type cylindrical cavities have been constructed for operating frequencies of 95 GHz

[4] and 140 GHz [39]. At higher frequencies, open-structured Fabry-Pérot (FP) resonators are used in HF-EPR instead of closed fundamental cavities [4, 5, 7, 9, 11, 40, 41]. FP resonators offer the advantage of relatively easy alignment and high quality factor due to their larger size and open structure. On the other hand, they are inferior to fundamental-mode cavities with respect to MW power conversion and sample filling factors. Also, sample handling is often difficult with FP resonators, since their planar or spherical MW field distribution prevents the use of cylindrical sample tubes.

For frequencies of up to 100 GHz, the full range of conventional MW components is available. These include MW circulators, variable attenuators and fast MW PIN switches. However, all these components decrease in their performance and become more fragile at higher MW frequencies, so they are not very convenient for use at frequencies above D-band (140 GHz). Also, the fundamental waveguides become increasingly lossy (7.2 dB/m at 180 GHz). Instead, quasi-optical (QO) components can be used for an efficient MW transmission from the source to the sample and back onto the receiver [2, 42, 43]. Far-infrared lasers can be used as MW sources at high frequencies [3, 6, 11, 44] but it is difficult to achieve specifications where the amplitude-, frequency- and phase-noise of these sources do not degrade the performance of the spectrometer. Hot-electron bolometers can be used as highly sensitive MW receivers at high frequencies, but normally their response time excludes them from the use for pulsed HF-EPR applications.

At present, superconducting solenoids are available for magnetic fields of up to about 20 T, corresponding to an MW frequency of 560 GHz for  $g = 2$ . Resistive magnets, which are able to produce much larger static or pulsed magnetic fields have more restrictions for EPR applications and are installed only in a few high-field laboratories.

## 2 Experimental

### 2.1 Overall Description of the Spectrometer

A simplified scheme of the 180 GHz EPR spectrometer is shown in Fig. 4. On the top, the MW components are divided into two sections (a and b), summarizing the excitation and the detection channels of the heterodyne spectrometer with internal MW frequencies of 45–180 GHz (a) and 3–84 GHz (b), respectively. A doublexing circuit to the cavity is built of QO components and is shown in section (c), acting as a highly efficient MW circulator and variable MW attenuator at 180 GHz. MW propagation to the cavity is achieved by oversized rectangular waveguides (WR-28) and corresponding tapered transitions. The MW probe including the cylindrical cavity, which is of the fundamental  $TE_{011}$  mode [45], is discussed in more detail below. It is hosted in an integrated cryostat being part of the superconducting cryomagnet system (Teslatron, Oxford Instruments) with temperature control, which allows EPR measurements in the range from 4 to 300 K.

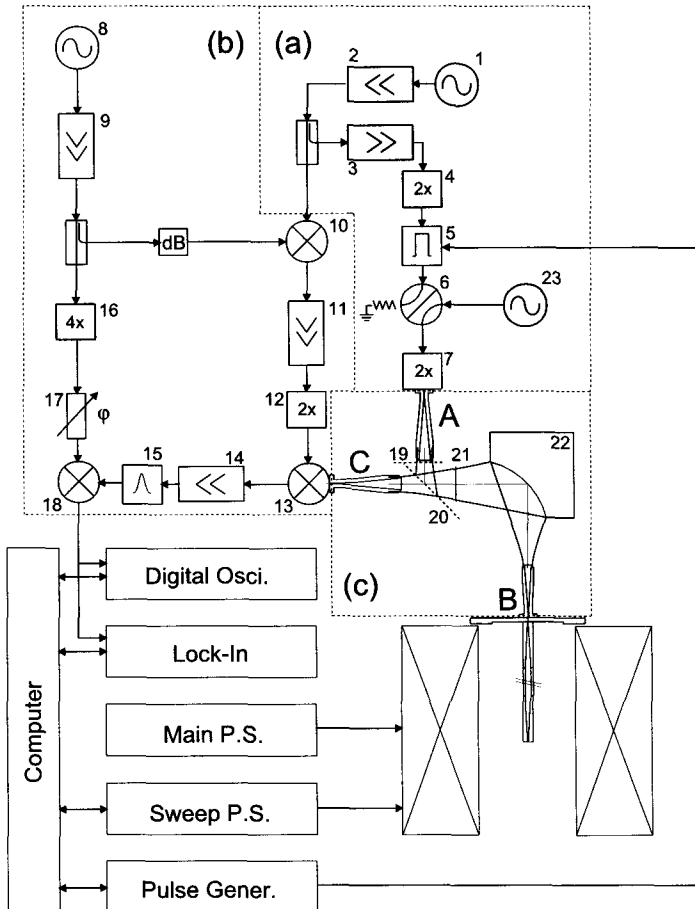


**Fig. 4.** Simplified scheme of the 180 GHz spectrometer. 1 – cavity-stabilized Gunn oscillator operating at  $45.000 \pm 0.075$  GHz, whose frequency can be mechanically adjusted, 2 – amplifier, providing 41 dBm power, 3 – four-stage injection locked oscillator (ILO) amplifier, providing 30 dBm, 4 – frequency doubler, 5 – MW PIN switch for pulsed experiments, 6 – mechanical waveguide switch, 7 – frequency doubler providing 15 dBm at 180 GHz, 8 – 3 GHz dielectric resonator oscillator (DRO), 9 – amplifier, 10 – mixer producing a frequency of 42 GHz, 11 – amplifier, 12 – frequency doubler to 84 GHz, 13 – subharmonic detection mixer producing a signal frequency of 12 GHz, 14 – low-noise amplifier, 15 – bandpass filter (bandwidth, 200 MHz), 16 – frequency multiplier, 17 – variable phase shifter, which can be adjusted mechanically, 18 – mixer with dc-200 MHz output, 19 – turnable polarizer grid serving as a variable attenuator, 20 – free standing polarizer grid, 21 – Faraday rotator, 22 – elliptical mirror, 23 – tuneable W-band Gunn diode oscillator. The capital letters A to C indicate the corrugated feed horns as described in the text. The sections a, b and c indicate the main transmitter channel, the detection channel and the QO components as explained in the text, respectively.

Experiment control and data acquisition are done by a PC and by means of a homewritten LabView program. It controls the home-built sweep coil power supply and a lock-in amplifier for CW experiments. Additionally, for pulsed EPR

experiments, a pulse generator (Sony/Tektronix DG 2020) is controlled by the computer program, as well as a digital oscilloscope (Tektronix TDS 520C) for the accumulation of the echo signals.

## 2.2 Magnet

The magnet system consists of two superconducting solenoids, one of which generates a static magnetic field in the range of 0–7 T. It can be locked in persistent mode and the current leads can be removed to decrease liquid helium consumption. In addition, the system contains a superconducting sweep coil. This produces magnetic fields of  $\pm 0.08$  T, corresponding to a DC current of  $\pm 25$  A. The home-built power supply for the sweep coil is controlled by a PC via a serial port and has a resolution of 18 bit (corresponding to  $0.61 \mu\text{T}$ ). The sweep coil exhibits a hysteresis effect of about 3.5 mT. To avoid nonlinearity of the magnetic field due to the hysteresis effect, field-dependent measurements have to start at least 15 mT prior to the first signal. The field homogeneity was specified and tested with an NMR probehead to be better than 2 ppm in a sphere with a radius of 5 mm around the center field. Included in the magnet system is a variable temperature insert (VTI, Oxford Instruments), which has a warm bore diameter of 74.2 mm. The temperature can be set with a temperature control unit (ITC503, Oxford Instruments) in the range of 4–300 K. For cooling the probe head, liquid helium from the reservoir of the magnet is evaporated into the VTI by means of a needle valve.

## 2.3 MW Generation and Detection

The MW generation and detection scheme is of the heterodyne type. The transmitter and the detection channel are indicated in sections a and b of Fig. 4, respectively. The MW source for the transmitter (and receiver) channel is a cavity-stabilized Gunn oscillator operating at a frequency of 45 GHz. Its frequency can be adjusted mechanically by means of a micrometer screw within a frequency range of  $\pm 75$  MHz, which corresponds to  $\pm 0.3$  GHz at the final operating frequency of 180 GHz. The transmitter channel includes a four-stage InP-injection locked oscillator (ILO) amplification, delivering 30 dBm MW power at 45 GHz. After conversion to 90 GHz by means of a high-power frequency doubler, we obtain about 25 dBm of MW power. At this point, fast MW switching is achieved by a PIN-diode switch, and thereafter a final frequency doubler provides the operation frequency of 180 GHz at an MW power of about 15 dBm in pulsed and CW mode. The last frequency doubler is directly attached to a corrugated feed horn (A in Fig. 4) where the mode conversion to a Gaussian beam is performed.

For the implemented heterodyne phase-sensitive detection scheme, a second MW source has to be used, which in our case is a dielectric resonator oscillator

(DRO) operating at a frequency of 3 GHz. This frequency can also be mechanically adjusted. After amplification, the MW power is split into two subchannels. The local (LO) frequency of 84 GHz for the final subharmonic detection mixer is generated in two steps by downconverting the 45 GHz signal from the same source as is used in the transmitter channel (see above) with one of the 3 GHz channels provided by the DRO, thus delivering a 42 GHz signal. An ILO amplifies the power of this signal before it is finally doubled to 84 GHz, which is used as the subharmonic LO frequency for the final detection mixer. In parallel to this high-frequency LO channel, the second low-frequency LO channel (on the left of section b, Fig. 4) is fed with the 3 GHz signal, which is multiplied to 12 GHz with a frequency multiplier chain, followed by a phase shifter.

The first step in the detection of the 180 GHz EPR signal is done by a subharmonically pumped 180 GHz mixer, which is connected directly to the corrugated feed horn C. Mixed with the second harmonic of the high-frequency LO channel of 84 GHz the EPR signal is downconverted to an intermediate signal frequency (IF) of 12 GHz, which is first amplified by a low-noise 12 GHz amplifier with a detection bandwidth of  $\Delta f = 200$  MHz and finally mixed in a second step with the low-frequency LO signal in a double-balanced mixer detector. This phase-sensitive output IF signal is further amplified or directly fed into a digitizing oscilloscope.

For monitoring and tuning of the cavity mode, a broadband Gunn diode oscillator is implemented into the system, which is connected to the last frequency doubler of the transmitter channel by means of a mechanical waveguide switch. The operating frequency of the Gunn diode oscillator can be swept between 85.8 and 91.2 GHz. For the detection of the reflected MW signal from the cavity a broadband 180 GHz diode detector is connected directly to horn C instead of the subharmonic detection mixer.

#### *2.4 Quasioptical Components*

As mentioned in Sect. 1, conventional three-port MW circulators operating at 180 GHz are not available. Consequently, we have included a relatively simple, but very efficient configuration of QO components that are summarized in section c of Fig. 4. It contains three corrugated feed horns numbered A through C. Horns A and C are identical and act as input and output ports. These horns are directly attached to the 180 GHz output port of the final frequency doubler (horn A) and to the RF port of the 180 GHz mixer detector (horn C). Thus, horn A converts the transmitted MW beam from the rectangular output (WR-05) to a free space Gaussian beam that is linearly polarized according to the vertical orientation of the 180 GHz doubler. First, the Gaussian beam passes through a rotatable polarizer grid. By varying the orientation of the polarizer grid, the amount of transmitted and reflected MW power can be adjusted continuously, so that the polarizer grid can serve as a very efficient variable attenuator with negligible transmission losses. After passing through this first polarizer grid, the transmit-

ted Gaussian beam is reflected by a vertically oriented polarizer grid, followed by a  $45^\circ$  Faraday rotator, which twists the polarization direction of the MW beam clockwise by  $45^\circ$  with respect to the propagation direction. The beam is then reflected by an elliptical mirror, which refocusses the MW beam into horn B positioned on top of the flange of the probehead. Horn B is followed by a rectangular tapered waveguide transition, converting the linear fundamental waveguide dimension of WR-05 to the oversized WR-28. Only one linear polarization direction is supported by the rectangular waveguide inside the probehead. At the bottom of the probehead, the cylindrical MW cavity is attached to a second tapered transition, which transfers the oversized WR-28 back to the fundamental WR-05. When the resonance condition is fulfilled, the reflected MW power from the cavity is transferred with the same linear polarization direction as the transmitted MW beam, as in typical, conventional, reflection-mode spectrometers and different from the so-called induction-mode detection scheme used in HF-EPR spectrometers with FP cavities and circular MW polarization for detection [5, 44]. In this reflection direction of propagation, the signal beam travels back through horn B and is reflected by the elliptical mirror. Passing through the Faraday rotator, its linear polarization direction is now twisted counterclockwise around  $45^\circ$  with respect to the propagation direction, thus being perpendicular to the initially transmitted beam. The horizontal polarization leads to an almost perfect transmission through the polarizer grid and refocusing of the signal beam into horn C. Consequently, the RF port of the 180 GHz mixer is oriented horizontally and allows for the effective conversion of the signal beam.

### 2.5 MW Cavity

The MW cavity is of the cylindrical  $TE_{011}$  mode [45], which leads to an inner diameter and a length of 2.2 mm, respectively, for a resonance frequency of 180 GHz. It is attached to a rectangular tapered transition that converts the oversized waveguide (WR-28) to the fundamental-mode dimensions of WR-05. In Fig. 5 details of the cavity and its MW coupling are depicted. MW coupling from the waveguide is done by means of a central coupling iris on top of the horizontally oriented cavity. The coupling can be varied during an EPR experiment at any time and temperature by the principle described previously for W-band (95 GHz) cavities [4], but with an improved mechanical adjustment. The effective diameter of the iris is variable by inserting a silver-coated tip into the coupling hole. The vertical position of the metal sphere is remotely controlled by means of the mechanism shown in Fig. 5. It is characterized by a dielectric plate, inserted into the short fundamental waveguide symmetrically from two opposite sides into the slotted waveguide section. The dielectric plate is fixed into a sliding holder on both sides, thus preventing the metal sphere from moving in any horizontal direction. The sliding holder is guided by means of four vertical cylindrical rods that are many wavelengths away from the cavity. Their positions are fixed to the holder and they are guided by eight sliding holes, four of each above and

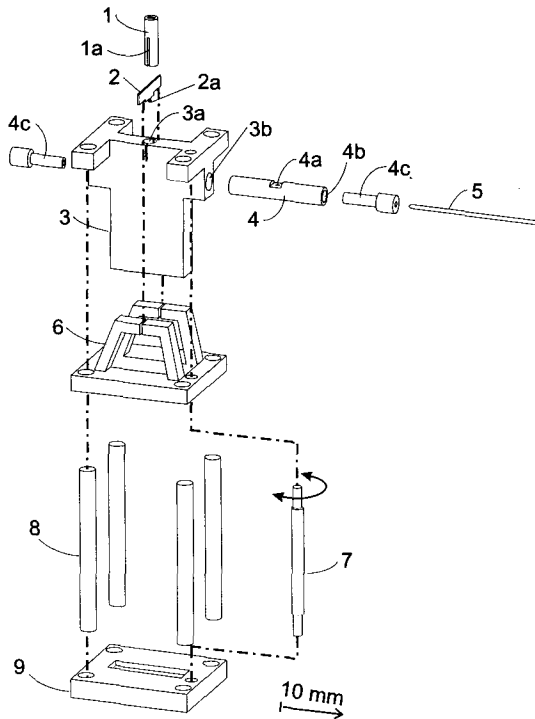


**Fig. 5.** 180 GHz MW resonator is shown in detail. 1 – fundamental waveguide, 1a – slit, which fits the dielectric plate, 2 – dielectric plate made out of teflon, 2a – silver-coated tip, 3 – main body with holes for introducing the waveguide (3a) and the cavity (3b), 4 – cavity, which can be removed for easy exchange, 4a – iris for the MW coupling, 4b – side holes for introducing the pistons, one of which is remotely controlled, 5 – sample tube, 6 – sliding block, which can be remotely controlled by use of the threaded bolt (7), 8 – guiding rods for the sliding block, 9 – ground plate.

below the cavity holder. Thereby, precise and stable movements of the coupling shifter are guaranteed, and as desired exclusively in the vertical direction. Remote control of the coupling mechanism is done by a fine-threaded screw drive that is also shown in Fig. 5.

Frequency tuning of the cavity is also possible during an EPR experiment by means of horizontally shifting one of the cavity pistons and thus changing the effective length of the cavity. A short lever transmits small angle rotation of a control rod to linear piston movements. The control rod is rotatable by another lever and a micrometer screw, both being positioned outside the probehead on its upper flange. The opposite, second cavity piston can be adjusted outside the magnet before starting the experiment. It also acts as the main sample holder by means of an axial hole that should be adjusted to the respective capillary diameter.

For performing CW experiments, modulation coils surround the cavity in a Helmholtz geometry. To reduce microphonics the modulation coils are connected

to the upper flange by means of three rods, which are mechanically disconnected from the other three rods, which hold the cavity and all other parts of the probe-head like the oversized waveguide or the remote-control mechanisms. In this way, the mechanical coupling between the modulation coils and the cavity is reduced to a minimum.

### *2.6 Experiment Control and Data Acquisition*

The homebuilt power supply for the sweep coil is connected to a computer via a serial port. All other devices (lock-in amplifier for CW detection, a digital oscilloscope for signal acquisition in the pulsed mode, and a pulse programmer used for forming the pulse sequences) are controlled via an IEEE bus. CW and pulsed EPR experiments are controlled by a homewritten LabView program running on an Intel Pentium 200 MHz PC.

## **3 Performance**

### *3.1 Quasioptics*

As mentioned above, QO components have been integrated into the MW transmission pathway due to the lack of conventional circulators and variable attenuators operating at 180 GHz. For a single pass from horn A to horn B (as indicated in Fig. 4) the insertion loss of the QO components is about 1.4 dB. While the insertion loss of the QO variable attenuator is negligible, the Faraday rotator exhibits an insertion loss of 0.7 dB. The remaining losses are caused by cross-polarization of the MW radiation, which is not reflected by the polarizer grid, and misalignment of the optical components. For comparison, a conventional circulator operating at 140 GHz has an insertion loss of 2.0 dB and a direct reading attenuator operating at W-band frequencies an insertion loss of 1.0 dB [46]. This comparison demonstrates the efficiency of the QO setup. Between horn B and the cavity the MW is transmitted via a WR-28 waveguide, which is connected to horn B and the cavity by means of two tapered transitions transferring the fundamental WR-05 waveguide to the oversized WR-28. While the MW losses of our setup are 0.8 dB for the oversized waveguide including both transition tapers attached, the losses of a fundamental WR-05 waveguide of the same length would be about 5 dB. The insertion loss for the complete setup is about 2.5 dB for a single pass from horn A to the cavity and 2.3 dB back from the cavity to the output flange of horn C, which is connected to the 180 GHz detection mixer. For comparison, the insertion loss including a conventional MW circulator and pathway is 8–9 dB at 140 GHz [39].

At short wavelengths, standing waves become a more serious issue in reflection-mode setups and unwanted reflections have to be reduced carefully. The remaining standing waves can be seen in Fig. 6, where the frequency-dependent

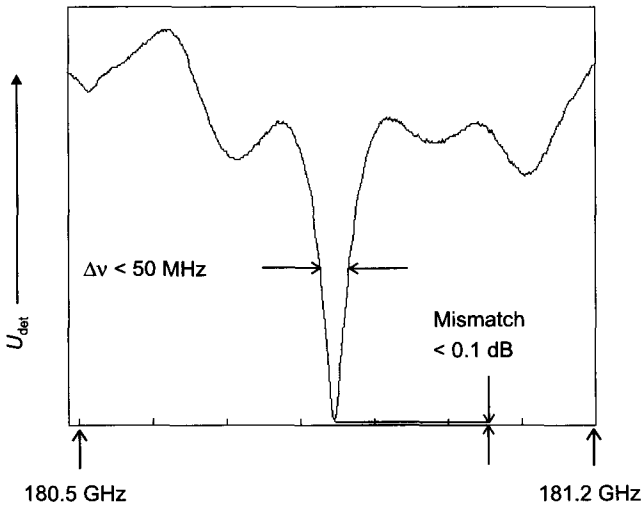


**Fig. 6.** Cavity mode showing the coupling of the cavity, the mismatch and the quality factor of  $Q \approx 4000$ . Also the standing waves of the transmission pathway as explained in the text can be seen.

MW response of the reflection setup including the cavity is shown. The periodicity of the standing waves can be assigned to the distance between the two tapered transitions. The standing waves may cause problems for tuning the MW coupling to the cavity as well as its resonance frequency, since tuning the cavity resonance into a minimum of the standing wave pattern significantly reduces the effective MW coupling. Standing waves in the transmission pathway may be reduced in the future by means of an oversized circular corrugated waveguide for transmitting the MW radiation from horn B to the cavity.

### 3.2 Cavity

Our 180 GHz EPR spectrometer can be run with high performance in CW and in pulsed mode without any alterations or adjustments to the probehead. In contrast to pulsed EPR experiments at lower frequencies, there is no need to reduce the quality factor of the cavity in order to shorten the deadtime caused by cavity ringing with a time constant given by the inverse of the excitation bandwidth of the cavity.

Due to the difficulties of determining the sample filling factor experimentally, only an estimation will be given here, following the description of Poole [45]. The sample filling factor is defined as

$$\eta = \frac{V_s \langle B_1^2 \rangle_s}{V_C \langle B_1^2 \rangle_C}, \quad (1)$$

with the indices S and C describing the sample and the cavity, respectively.  $V$  is the volume, and  $B_1$  is the oscillating magnetic field inside the cavity. If a sample tube is inserted into the full length of a cylindrical cavity with the given dimensions operating in the  $TE_{011}$  mode, the filling factor can be estimated to  $\eta = 0.09$  for a sample tube with an inner diameter of 0.3 mm. For sample tubes with inner diameters of 0.4 and 0.5 mm the filling factor increases to 0.16 and 0.25, respectively.

### 3.3 Spectrometer Performance

The CW sensitivity of the spectrometer is determined experimentally to be in the range of  $10^{10}$  spins/(mT·Hz<sup>1/2</sup>). The overall noise figure of the detection channel is dominated by the noise figure of the first detection mixer, which is specified to be better than 9 dB. Including the noise figures and conversion gains or losses of all following components in the detection channel as well as the MW losses of the QO transmission pathway, an overall noise figure  $F$  of about 13 dB is estimated. These values are in the range of other HF-EPR spectrometers operating at 95, 140 and 250 GHz with reported CW sensitivities of  $4 \cdot 10^8$ ,  $1.4 \cdot 10^9$  and  $10^{12}$  spins/(mT·Hz<sup>1/2</sup>) [10, 39, 47].

The overall theoretical sensitivity of a CW EPR spectrometer is given by [48]:

$$N^* = \frac{c_1 (kT)^{3/2} V_s}{Q \eta B_0} \sqrt{\frac{F \Delta f}{P_0}}, \quad (2)$$

where  $\Delta f$  is the detection bandwidth,  $F$  the noise figure of the detection channel,  $Q$  the quality factor of the loaded cavity,  $P_0$  the excitation power,  $B_0$  the external magnetic field,  $V_s$  the sample volume,  $\eta$  the filling factor, and  $c_1$  is given by

$$c_1 = \frac{1}{\mu_0 g^2 \beta_e^2 S(S+1)}, \quad (3)$$

where the constants have their common meaning. This expression leads to a theoretical sensitivity which is about two orders of magnitude better than the measured sensitivity given above. This can be due to two other sources of noise for a CW EPR experiment which are neglected in Eq. (2): the noise of the MW source, which is mostly determined by the phase and frequency noise of the 45 GHz cavity stabilized Gunn oscillator and its power amplification chain, and the microphonic noise introduced by the field modulation coils. Both effects gain increased importance at higher MW frequencies. At higher magnetic fields and smaller cavity dimensions the mechanical decoupling of the modulation coil from the cavity becomes rather difficult: whereas larger modulation amplitudes have to be used because of the increased spectral width, the sensitivity of the cavity to mechanical vibrations is strongly enhanced. The spectral purity of the MW

source is also reduced compared to lower frequency MW sources. In many cases the high-frequency MW source is phase-locked to a high harmonic of a low-frequency quartz oscillator. In this case the spectral performance of the low-frequency quartz oscillator is reduced by the harmonic multiplication factor. In our setup, where the MW source is optimized for maximum output power for pulsed EPR operation the situation is even worse: the cavity-stabilized oscillator as well as the injection-locked oscillator amplifiers introduce additional noise into the excitation and LO port of the detection channel which are not cancelled by the heterodyne mixing scheme.

Quite in contrast, pulsed performance of an EPR spectrometer is mostly affected by the pulse lengths. These are functions of the available MW power  $P_0$ , the conversion factor  $c$  of the cavity and of the quality factor  $Q$  of the cavity:

$$t_p^{-1} \propto B_1 = c\sqrt{QP_0}, \quad (4)$$

$t_p$  is the pulse length and  $B_1$  the excitation field strength inside the cavity. For obtaining pulses as short as possible, the magnetic field strength  $B_1$  has to be as high as possible.

While the MW input power is given by the maximum source power and the insertion losses of the transmission pathway, the other two parameters can be optimized by the design and the mechanical matching of the cavity and the MW coupling to it.

The conversion factor  $c$  of the cavity is a function of the MW frequency:

$$c \propto \sqrt{\frac{\mu_0}{V_C v_0}} \approx v_0 \sqrt{\mu_0}, \quad (5)$$

with  $V_C$  being the cavity volume,  $v_0$  the MW frequency and  $\mu_0$  the vacuum permeability. Compared to a similar cavity operating at W-band frequencies, whose conversion factor is in the range of  $50 \mu\text{T}/\text{W}^{-1/2}$  [10], a conversion factor of about  $100 \mu\text{T}/\text{W}^{-1/2}$  would be expected for our cavity due to the higher frequency. In fact, the achieved conversion factor of  $30 \mu\text{T}/\text{W}^{-1/2}$  is a factor of 3 smaller as compared to the expected value, which is most probably caused by the small sizes of the mechanical parts and the cavity compared to the inserted sample and sample capillary. Most probably this leads to larger distortions of the calculated ideal MW distribution inside the loaded cavity for larger frequencies and smaller dimensions. This effect can also be seen for a similar cavity operating at 140 GHz, whose conversion factor is of about  $40 \mu\text{T}/\text{W}^{-1/2}$  [49]. Therefore this comparison suggests that a threshold around 100 GHz may exist for this type of cavity, above which the achieved conversion factor does not improve any more.

With these values, typical  $\pi/2$  pulse lengths of ca. 60 ns are achieved. The limiting sources of noise for CW EPR sensitivity at high MW frequencies discussed above, microphonics and source noise, do not enter into the sensitivity

of pulsed EPR applications. We performed a comparison of the signal-to-noise ( $S/N$ ) ratio for a single-shot two-pulse echo signal of a small  $\alpha,\gamma$ -bisdiphenylene- $\beta$ -phenylallyl benzolate sample at 180 and 9 GHz MW frequency. Correcting for the different effective sample sizes and excitation bandwidths the experimental observed enhancement in  $S/N$  for small samples with narrow linewidth (as for example single crystal of protein samples) is:

$$E_{\text{GX}} = \frac{S/N(180 \text{ GHz})}{S/N(9 \text{ GHz})} \approx 40, \quad (6)$$

this value is comparable to the gain obtained at W-band frequencies and only a factor of 7 lower than the theoretical expected enhancement calculated with the experimental parameters and given by [50]:

$$S/N \sim \frac{\sqrt{Q}v_{\text{MW}}^{3/2}}{\sqrt{V_c F \Delta f (kT)^3}}. \quad (7)$$

The difference to the theoretically calculated enhancement is probably due to the same reasons limiting the conversion factor of the cavity, leading to a decreased  $B_1$  field strength and field homogeneity at the sample. Nevertheless the experimentally reached value is close to the predicted enhancement, demonstrating the less demanding requirements for pulsed HF-EPR applications as compared to CW EPR. Therefore, pulsed HF-EPR has a dramatically enhanced sensitivity for small single-crystal samples [10, 33].

**Table 1.** Technical data of our pulsed 180 GHz spectrometer.

Operating MW frequency $\nu_{\text{MW}}$	180.0 ± 0.3 GHz
Magnet (Oxford Instruments)	$B_0 \leq 7$ T
$B_0$ field main coil at $g = 2$	6.422 T
$B_0$ sweep range (supercond. sweep coil)	± 0.08 T
$B_0$ homogeneity (in a sphere with 0.5 cm radius)	≤ 2 · 10 <sup>-6</sup>
Temperature range	4–300 K
MW resonator type	cylindrical, TE <sub>011</sub>
Cavity dimensions	2.2 mm length, 2.2 mm diameter
MW coupling	variable iris coupling
MW conversion factor $c$	0.03 ± 0.01 mT/W <sup>1/2</sup>
Sample filling factor $\eta$	0.09–0.25
MW output power at 180 GHz $P_{\text{MW}}$	≈ 15 dBm
MW power incident to resonator $P_0$	≈ 12 dBm
$\pi/2$ -pulse length $t_p$	≈ 60 ns
MW switching on-off isolation (at 90 GHz)	47 dB
MW pindiode switching speed	≤ 5 ns
Noise figure $F$ of detection at 180 GHz	≈ 13 dB
CW sensitivity $N^*$	10 <sup>10</sup> spins/(mT · Hz <sup>1/2</sup> )
Pulsed sensitivity gain $E_{\text{GX}} = (S/N)_{\text{G}}/(S/N)_{\text{X}}$	40

Table 1 summarizes all the relevant technical data describing the performance of our 180 GHz spectrometer.

#### 4 Summary

We describe an EPR spectrometer operational in pulsed as well as CW mode at an MW frequency of 180 GHz. The miniaturized cylindrical MW cavity permits the use of commercial quartz capillaries as sample holders. The partial use of QO MW components in conjunction with the ten times higher conversion factor of the cylindrical cavity as compared to Fabry-Pérot resonators allows one to perform pulsed EPR experiments even with only moderate MW power with a reasonable spectrometer performance. While the performance of the spectrometer with respect to CW sensitivity is not as high as theoretically predicted, the pulsed sensitivity meets the expectations very well. Both sensitivities are comparable with other homebuilt HF-EPR spectrometers. The hybrid architecture of the spectrometer, including QO MW components exclusively to replace a conventional MW circulator and an attenuator at 180 GHz, has thereby proven a very successful concept for EPR spectrometers at MW frequencies around 200 GHz. The extension of the spectrometer to ENDOR capability is currently under way, as are applications on biological samples as shown in Figs. 1 to 3.

#### Acknowledgements

We gratefully acknowledge Mr. Jäger, Mr. van Tankeren and Mr. Eimer from the mechanical workshop of our institute, who helped to develop the mechanical parts of the probehead. Mr. Zimmermann and Mr. Rose from Radiometer Physics GmbH designed the QO components. Mr. Cutsinger from Millimeter-Wave Oscillator Company designed the MW transmitter and receiver system. M. Spoerner is thanked for the Ras protein complex, whose CW spectrum at 2.9 GHz was recorded by A. Weber, and the W-band measurement was performed by Dr. H. Käß in the research group of Prof. K.-P. Dinse at the Technical University of Darmstadt. T. Kretz and Dr. F. MacMillan are thanked for the vitamin K<sub>3</sub> sample and its X-band spectrum.

This work was supported by the Deutsche Forschungsgemeinschaft (Schwerpunktprogramm "Hochfeld EPR in Biologie, Chemie und Physik") and by the country of Hesse (HBFVG).

#### References

1. Grinberg O.Y., Dubinski A.A., Lebedev Y.S.: *Russ. Chem. Rev.* **52**, 850–865 (1983)
2. Lynch W.B., Earle K.A., Freed J.H.: *Rev. Sci. Instrum.* **59**, 1345–1351 (1988)
3. Muller F., Hopkins M.A., Coron N., Grynberg M., Brunel L.-C., Martinez G.: *Rev. Sci. Instrum.* **60**, 3681–3684 (1989)
4. Burghaus O., Rohrer M., Götzinger T., Plato M., Möbius K.: *Meas. Sci. Technol.* **3**, 765–774 (1992)

5. Fuchs M.R., Prisner T.F., Möbius K.: *Rev. Sci. Instrum.* **70**, 3681–3683 (1999)
6. Hassan A.K., Pardi L.A., Krzystek J., Sienkiewicz A., Goy P., Rohrer M., Brunel L.-C.: *J. Magn. Reson.* **142**, 300–312 (2000)
7. Weber R.T., Disselhorst J.A.J.M., Prevo L.J., Schmidt J., Wenckebach W.T.: *J. Magn. Reson.* **81**, 129–144 (1988)
8. Bresguenov A.Y., Dubinski A.A., Krimov V.N., Petrov Y.G., Poluetkov O.G., Lebedev Y.S.: *Appl. Magn. Reson.* **2**, 715–728 (1991)
9. Prisner T.F., Un S., Griffin R.G.: *Isr. J. Chem.* **32**, 357–363 (1992)
10. Prisner T.F., Rohrer M., Möbius K.: *Appl. Magn. Reson.* **7**, 167–183 (1994)
11. Kutter C., Moll H.P., van Tol J., Zuckermann H., Maan J.C., Wyder P.: *Phys. Rev. Lett.* **74**, 2925–2928 (1995)
12. van Dujin-Arnold A., Mol J., Verberk R., Schmidt J., Mokhov E.N., Baranov P.G.: *Phys. Rev. B* **60**, 15829–15847 (1999)
13. Barra A.-L., Debrunner P., Gatteschi D., Schulz C.E., Sessoli R.: *Europhys. Lett.* **35**, 133–138 (1996)
14. Pilawa B., Kelemen M.T., Wanka S., Geisselmann A., Barra A.-L.: *Europhys. Lett.* **43**, 7–12 (1998)
15. Hagen W.R.: *Coord. Chem. Rev.* **190–192**, 209–229 (1999)
16. Gaffney B.J., Maguire B.C., Weber R.T., Maresch G.G.: *Appl. Magn. Reson.* **16**, 207–222 (1999)
17. Käss H., MacMillan F., Ludwig B., Prisner T.F.: *J. Phys. Chem. B* **104**, 5362–5371 (2000)
18. van Gastel M., Canters G.W., Krupka H., Messerschmidt A., de Waal E.C., Warmerdam G.C.M., Groenen E.J.J.: *J. Am. Chem. Soc.* **122**, 2322–2328 (2000)
19. Rohrer M., Prisner T.F., Brüggemann O., Käss H., Spoermer M., Wittinghofer A., Kalbitzer H.-R.: *Biochemistry* **40**, 1884–1889 (2001)
20. Burghaus O., Plato M., Rohrer M., Möbius K., MacMillan F., Lubitz W.: *J. Phys. Chem.* **97**, 7639–7647 (1993)
21. Prisner T.F., McDermott A.E., Un S., Norris J.R., Thurnauer M.C., Griffin R.G.: *Proc. Natl. Acad. Sci. USA* **90**, 9485–9488 (1993)
22. Un S., Atta M., Fontecave M., Rutherford A.W.: *J. Am. Chem. Soc.* **117**, 10713–10719 (1995)
23. Gerfen G.J., Bellew B.F., Un S., Belling J.M., Stubbe J., Griffin R.G., Singel D.J.: *J. Am. Chem. Soc.* **115**, 6420–6421 (1993)
24. Dorlet P., Rutherford W.A., Un S.: *Biochemistry* **39**, 7826–7834 (2000)
25. Goldberg D.P., Telser J., Krzystek J., Montalban A.G., Brunel L.-C., Barrett G.M., Hoffman B.M.: *J. Am. Chem. Soc.* **119**, 8722–8723 (1997)
26. Prisner T.F. in: *Advances in Magnetic and Optical Resonance* (Warren W.S., ed.), vol. 20, pp. 245–299. San Diego: Academic Press 1997.
27. Schweins T., Scheffzek K., Abheuer R., Wittinghofer A.: *J. Mol. Biol.* **266**, 847–856 (1997)
28. Rohrer M., Plato M., MacMillan F., Grishin Y., Lubitz W., Möbius K.: *J. Magn. Reson. A* **116**, 59–66 (1995)
29. Rohrer M., MacMillan F., Prisner T.F., Gardiner A.T., Möbius K., Lubitz W.: *J. Phys. Chem. B* **102**, 4648–4657 (1998)
30. Rohrer M., Gast P., Möbius K., Prisner T.F.: *Chem. Phys. Lett.* **259**, 523–530 (1996)
31. Prisner T., Rohrer M., MacMillan F.: *Annu. Rev. Phys. Chem.* **52**, 279–313 (2001)
32. Bloß A., Möbius K., Prisner T.F.: *J. Magn. Reson.* **134**, 30–35 (1998)
33. Coremans J.W.A., Poluetkov O.G., Groenen E.J.J., Canters G.W., Nar H., Messerschmidt A.: *J. Am. Chem. Soc.* **119**, 4726–4731 (1997)
34. Manikandan P., Carmieli R., Shane T., Kalb A.J., Godfarb D.: *J. Am. Chem. Soc.* **122**, 3488–3494 (2000)
35. Liang Z., Freed J.H.: *J. Phys. Chem. B* **103**, 6384–6396 (1999)
36. Bennati M., Gerfen G.J., Martinez G.V., Griffin R.G., Singel D.J., Millhauser G.L.: *J. Magn. Reson.* **139**, 281–286 (1999)
37. Barnes J.P., Liang Z., Mchaourab H.S., Freed J.H., Hubbell W.: *Biophys. J.* **76**, 3298–3306 (1999)
38. Steinhoff H.-J., Savitzky A., Wegener C., Pfeiffer M., Plato M., Möbius K.: *Biochim. Biophys. Acta* **1457**, 253–262 (2000)
39. Bennati M., Farrar C.T., Bryant J.A., Inati S.J., Weis V., Gerfen G.J., Riggs-Gelasco P., Stubbe J., Griffin R.G.: *J. Magn. Reson.* **138**, 232–243 (1999)
40. Rohrer M., Krzystek J., Williams V., Brunel L.-C.: *Meas. Sci. Technol.* **10**, 275–284 (1999)
41. Barnes J.P., Freed J.H.: *Rev. Sci. Instrum.* **69**, 3022–3027 (1998)

42. Smith G.M., Lesurf J.C.G., Mitchell R.H., Riedi P.C.: *Rev. Sci. Instrum.* **69**, 3924–3937 (1998)
43. Earle K., Freed J.H.: *Appl. Magn. Reson.* **16**, 247–272 (1999)
44. Moll H.P., Cutter C., van Tol J., Zuckerman H., Wyder P.: *J. Magn. Reson.* **137**, 46–58 (1999)
45. Poole C.P.: *Electron Spin Resonance*. New York: Wiley 1967.
46. Millitech: *Millimeter-Wave Products, product catalogue*. Northampton, Mass.: Millitech 1995.
47. Earle K.A., Budil D.E., Freed J.H. in: *Advances in Magnetic and Optical Resonance* (Warren W.S., ed.), vol. 19, pp. 253–323. New York: Academic Press 1996.
48. Feher G.: *Bell Syst. Tech. J.* **36**, 449–484 (1957)
49. Becerra L.R., Gerfen G.J., Bellew B.F., Bryant J.A., Hall D.A., Inati S.J., Weber R.T., Un S., Prisner T.F., McDermott A.E., Fishbein K.W., Kreisler K.E., Temkin R.J., Singel D.J., Griffin R.G.: *J. Magn. Reson. A* **117**, 28–40 (1995)
50. Shaw D.: *Fourier Transform NMR Spectroscopy*. Amsterdam: Elsevier 1976.

**Authors' address:** Thomas F. Prisner, Institut für Physikalische und Theoretische Chemie, Universität Frankfurt, Marie-Curie Strasse 11, 60439 Frankfurt/Main, Germany